Applied Catalysis B: Environmental 148–149 (2014) 51–61

Contents lists available at ScienceDirect

Applied Catalysis B: Environmental

journal homepage: www.elsevier.com/locate/apcatb

Effect of aging on NO_x reduction in coupled LNT–SCR systems

Jin Wang, Yaying Ji, Gary Jacobs, Samantha Jones, Dae Jung Kim, Mark Crocker*

Center for Applied Energy Research, University of Kentucky, Lexington, KY 40511, USA

ARTICLE INFO

Article history:
Received 13 August 2013
Received in revised form 15 October 2013
Accepted 17 October 2013
Available online 25 October 2013

Keywords:
LNT–SCR
Lean NO_x trap
NO_x adsorber catalyst
Selective catalytic reduction
Catalyst aging

ABSTRACT

The effect of simulated road aging on the NO_x reduction performance of coupled Pt/Rh LNT and Cu-CHA SCR catalysts was studied using H_2, CO and C_3H_6 as NO_x reductants. Activity tests showed that the NO_x reduction activity of the LNT was significantly decreased after aging, especially at low temperature. N_2 physisorption, H_2 chemisorption, elemental analysis and TEM results revealed two main changes which account for the degradation in LNT performance. First, residual sulfur in the aged LNT associated with the Ba phase was responsible for decreased NO_x storage efficiency. Second, sintering of the precious metals in the washcoat occurred, resulting in decreased contact between the Pt and Ba, and hence in less efficient NO_x storage and catalyst regeneration. The aged LNT showed higher NH_3 selectivity than that of the fresh LNT in the temperature range 150–450 °C, NH_3 generated from the LNT being stored by the SCR catalyst which subsequently catalyzed its reaction with NO_x slip from the LNT. Hence, the loss of NO_x conversion over the LNT was partly compensated by the downstream SCR catalyst. N_2O formation over the aged LNT was less than that over the fresh LNT and the N_2O was partly mitigated by the downstream SCR catalyst. Microreactor tests further showed that in addition to NH_3, the SCR catalyst was able to use slipped CO or C_3H_6 as NO_x reductants. A comparison of the difference in NO_x conversion for the aged LNT and LNT–SCR configurations for the three reductants used in this study showed that the greatest benefit was obtained when CO and C_3H_6 were the reductants. This is explained by the fact that the LNT catalyst was unable to utilize these reductants as efficiently as H_2 due to their lower reactivity; hence, more NO_x and reductant slip reached the SCR catalyst. The ability of the SCR catalyst to utilize these reductants therefore provides a significant advantage over the LNT-only configuration.

1. Introduction

Lean-burn engines provide more efficient fuel combustion and lower CO_2 emissions compared with traditional stoichiometric engines. However, control of NO_x emissions is challenging because of the difficulty in reducing NO_x in lean exhaust conditions. Two main approaches to this problem have emerged in recent years in the form of lean NO_x traps (LNTs) and selective catalytic reduction (SCR). LNTs function by storing NO_x under lean conditions in the form of nitrate and/or nitrite; upon periodic short excursions to rich conditions, the stored NO_x is released and reduced to N_2. In contrast, SCR systems rely upon the catalyzed reaction of NO_x with externally added NH_3 in the presence of excess oxygen. In recent years, studies have shown that the NO_x reduction performance of lean NO_x trap (LNT) catalysts can be significantly improved by adding a downstream SCR catalyst [1–25]. In this configuration the SCR catalyst functions in an in situ mode, i.e., NH_3 generated from the LNT during rich purging can be stored on the SCR catalyst and then utilized to reduce NO_x slip through the LNT during subsequent lean operation. Hence, in the coupled LNT–SCR system, not only is the NO_x removal efficiency greatly increased but also the NH_3 slip is decreased. In addition, a second NO_x reduction pathway can operate when the SCR catalyst is of the Cu-CHA type, this pathway being associated with the presence of hydrocarbons which slip through the LNT catalyst in the rich phase and act as NO_x reductants [21,24]. Other benefits arising from the presence of the SCR catalyst include reduced emissions of N_2O (formed over the LNT) [26], a consequence of the activity exhibited by Cu-CHA for N_2O decomposition. Moreover, given that NO_x conversion can be partially shifted to the SCR catalyst, the LNT–SCR concept offers the potential for decreased usage of platinum group metals (PGMs) in the LNT, thereby lowering its cost [11,24]. This catalytic technology has been applied in the US and in Europe by Daimler AG [12].

Another potential benefit of the LNT–SCR concept is improved durability relative to LNT-only systems. In principle, the SCR catalyst can compensate for activity losses in the LNT resulting from aging by converting NO_x (and reductants) that slip through the LNT. Although LNT catalysts are applied commercially, the issue of catalyst durability remains problematic. Indeed, two main deactivation mechanisms have been recognized for LNTs [27–30], corresponding to (i) sintering of the PGMs, which results in phase segregation of the PGMs and the NO_x storage material (typically Ba), and (ii)

* Corresponding author. Tel.: +1 859 257 0295.
E-mail address: mark.crocker@uky.edu (M. Crocker).

0926-3373/$ – see front matter © 2013 Elsevier B.V. All rights reserved.
http://dx.doi.org/10.1016/j.apcatb.2013.10.037

the accumulation of sulfur in the NO_x storage material, not all of which is removed during periodic desulfation. These degradation pathways result in decreased catalyst efficiency for NO_x storage and release, as well as decreased activity for the reduction of released NO_x [27–30]. In contrast, Cu-CHA SCR catalysts are recognized for their high durability, particularly with respect to hydrothermal aging [31–33]. However, deactivation of Cu-CHA can occur upon severe aging via dealumination of the zeolite (eventually leading to collapse of the zeolite structure) and Cu sintering [34].

To date, few studies have appeared concerning the effect of aging on the performance of LNT–SCR systems. Seo et al. [35] examined the deNO_x characteristics of coupled Pt/Pd/Rh LNT and Fe-zeolite SCR catalysts using CO/H_2 as reductant, the LNT–SCR system being subjected to hydrothermal aging at 750 °C and 900 °C and, separately, sulfur poisoning. It was concluded that the SCR catalyst was indeed able to compensate the decreased activity of the LNT to a certain degree, as well as reducing the NH_3 slip. McCabe and co-workers [14,24] examined the performance of systems incorporating Fe-zeolite or Cu-zeolite catalysts and confirmed the ability of the SCR catalyst to compensate the decreased NO_x reduction activity of the LNT after aging. They also found that a minimally deactivated Cu-CHA catalyst downstream of the LNT can offset decreased LNT activity for hydrocarbon conversion due to aging [23].

The present study aimed to evaluate the performance of coupled Pt/Rh LNT and Cu-CHA SCR catalysts after simulated road aging. The NO_x reduction performance, NH_3 production and N_2O emissions from the LNT and from the coupled LNT–SCR system in the presence of different reductants (H_2, CO, and C_3H_6) are reported, and an effort is made to relate changes in catalyst performance after aging to changes in the structure of the catalysts.

2. Experimental

2.1. Catalysts

Two catalysts were used in this study, comprising a low-precious metal loaded Pt/Rh LNT catalyst and a commercial SCR catalyst of the Cu-chabazite type (Cu-SSZ-13). The LNT catalyst contained BaO as the main NO_x storage material, as well as a ceria-zirconia oxygen storage material, and Pt and Rh as the precious metals. Both catalysts were provided by BASF and were prepared on 400 cpsi/6.5 mil ceramic monoliths. For bench reactor tests, 3.8 cm (l) × 2.1 cm (d) core samples of each catalyst were drilled from the monoliths.

2.2. Aging protocol

Catalyst aging was performed on a synthetic gas bench using a rapid aging protocol which has been detailed in earlier papers [11,29]. The LNT and SCR catalysts were placed in the same reactor, the SCR catalyst being placed downstream of the LNT. Each aging cycle was composed of three modes: sulfation, desulfation, and simulated DPF regeneration, the corresponding feed gas compositions being shown in Table 1. Fig. 1 summarizes the protocol used for the accelerated catalyst aging. As described previously [29], the maximum mid-bed temperature experienced by the LNT catalyst occurs during the desulfation mode of the aging cycle and typically corresponds to 770 ± 10 °C, this being higher than the 700 °C set-point due to the exotherm created by lean-rich cycling. This is illustrated in Fig. S1, which depicts LNT catalyst inlet and mid-bed temperatures for one aging cycle. The corresponding maximum temperature experienced by the SCR catalyst downstream of the LNT was 750 ± 10 °C (inlet temperature). Depending on actual fuel sulfur levels, one aging cycle is estimated to be equivalent to 1000–1500 miles of road aging. In total, 50 cycles were used for the aging, requiring a total aging time of ca. 100 h. At the end of each aging run a final desulfation was performed under constant rich conditions, corresponding to 2% H_2 in the presence of 5% CO_2 and 5% H_2O at 750 °C for 10 min, in order to remove as much residual sulfur as possible.

Table 1
Composition of feed gas for LNT–SCR system aging.

Parameter	Sulfation		Desulfation		DPF regeneration
	Lean	Rich	Lean	Rich	
Duration (s)	60	5	5	15	1800
Temperature (°C)	300	300	700	700	650
NO (ppm)	300	300	300	300	0
O_2 (%)	8	0	8	0	8
CO (%)	–	4	0	4	0
H_2 (%)	0	1.3	0	1.3	0
SO_2 (ppm)	45	45	0	0	0
CO_2 (%)	5	5	5	5	5
H_2O (%)	5	5	5	5	5
N_2 (%)	Balance	Balance	Balance	Balance	Balance
Space velocity (h^{-1})	60,000	60,000	60,000	60,000	60,000

2.3. LNT–SCR lean-rich cycling experiments

Catalyst testing was performed on a synthetic gas bench. The LNT and SCR monolith cores were wrapped in Zetex insulation tape and placed in separate vertical reactor tubes (2.2 cm inner diameter) which were independently heated by two electric furnaces. Details concerning the reactor configuration and product analysis system can be found in a previous paper [21]. Briefly, the catalysts were positioned in series, the inlet face of the SCR catalyst monolith being 10" downstream of the outlet face of the LNT monolith. A gas sampling port was positioned between the catalysts to enable analysis of the effluent gas from the LNT catalyst. A rapid switching 4-way valve system was used to alternate between the lean and rich gas mixtures so that the lean/rich/lean transitions in these experiments were almost instantaneous (within 0.2 s). K-type thermocouples were placed at the LNT inlet, mid-point and exit, and the SCR catalyst inlet and outlet, to monitor the temperature profiles. Regulation of the catalyst temperature during experiments was based on the catalyst inlet temperature; consequently, all operating temperatures quoted in this work (i.e., in tables and figures) correspond to catalyst inlet temperatures. A multi-gas analyzer (MKS Model 2030) was used to monitor the concentrations of NO, NO_2, N_2O, NH_3, C_3H_6, CO, CO_2, and H_2O between the LNT and SCR

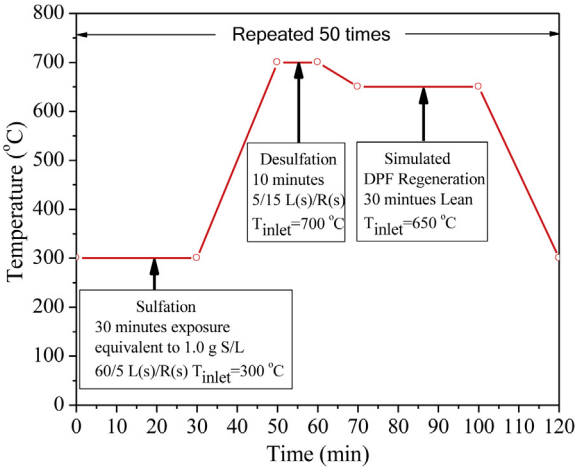

Fig. 1. Summary of protocol used for accelerated catalyst aging.

Table 2
Base conditions used for NO_x storage-reduction cycling experiments.

Parameter	Lean	Rich 1	Rich 2	Rich 3
Duration (s)	60	5	5	5
Temperature (°C)	150–450	150–450	150–450	150–450
NO (ppm)	300	0	0	0
H_2 (%)	0	2.5	0	0
CO (%)	0		2.5	0
C_3H_6 (ppm)	0	0		3333
CO_2 (%)	5	5	5	5
H_2O (%)	5	5	5	5
N_2 (%)	Balance	Balance	Balance	Balance
Space velocity (h^{-1})	60,000	60,000	60,000	60,000

catalysts, as well as at the inlet of the LNT and at the outlet of the SCR catalyst. During lean-rich cycling, the observed catalyst breakthrough profiles stabilized to a fixed limit cycle in about 2 h, at which point it was possible to characterize the performance in terms of the 'stationary' concentration cycles. Data were collected in the range 150–450 °C using the gas compositions summarized in Table 2. The selectivity to N_2O and NH_3 was calculated according to:

$$S_{N_2O}(\%) = 100 \times \frac{2\int_0^t [N_2O]dt}{\int_0^t ([NO_x]_0 - [NO_x])dt}$$

$$S_{NH_3}(\%) = 100 \times \frac{\int_0^t [NH_3]dt}{\int_0^t ([NO_x]_0 - [NO_x])dt}$$

The selectivity to N_2 was determined by difference, i.e., $S_{N_2} = 100\% - S_{NH_3} - S_{N_2O}$. NO_x conversion over the LNT and SCR catalysts during these experiments was calculated according to: NO_x conversion (%) $= 100 \times ([NO_x]_{inlet} - [NO_x]_{outlet})/[NO_x]_{inlet}$, where all concentrations are cycle-averaged, integrated values (in ppm s). In all cases, the average of five consecutive lean-rich cycles was used to calculate conversion and selectivity data. Before beginning the measurements catalysts were degreened under lean-rich cycling conditions at 500 °C for 5 h, using the lean gas feed and rich gas feed 1 shown in Table 2.

2.4. NO_x reduction experiments over SCR catalyst under continuous flow conditions

Experiments were performed in the synthetic gas bench reactor described above using a 3.8 cm (l) × 2.1 cm (d) core sample of the SCR catalyst. The total feed gas flow rate was set to 13,719 sccm, giving a GHSV of 60,000 h^{-1}. Two K-type thermocouples were placed just before the SCR catalyst and at the catalyst outlet to monitor the temperature profile. The catalyst was pre-treated in a flowing mixture of 8% O_2, 5% CO_2, 5% H_2O and N_2 (balance) at 500 °C for 3 h, after which the catalyst was cooled to 150 °C under a flowing feed of 5% CO_2, 5% H_2O and N_2 (balance). At this point NO_x (300 ppm), 300 ppm NH_3, and 8% O_2 were added to the feed. NO_x and NH_3 conversion measurements were performed under steady-state conditions at intervals of 50 °C in the temperature range 150–500 °C.

2.5. Catalyst characterization

Surface area and pore volume measurements were performed according to the BET method by nitrogen adsorption at −196 °C using a Micromeritics Tri-Star system. Prior to the measurements, catalysts (washcoat and monolith) were ground to a fine powder and outgassed overnight at 160 °C under vacuum. The amount of residual sulfur in the samples was measured by detecting the SO_2 evolved after heating the ground catalyst sample to 1425 °C using an ELTRA CS 500 Carbon Sulfur Determinator. Power X-ray diffraction (XRD) measurements were performed on a Phillips X'Pert diffractometer using Cu K(alpha) radiation (λ = 1.5406 Å) and a step size of 0.02°.

The dispersion of precious metal (Pt + Rh) was determined with a Micromeritics AutoChem II Analyzer by means of pulsed H_2 chemisorption at dry ice temperature (−78 °C). This temperature was chosen in an effort to minimize H spillover from the metal to the support material [30,36]. A quantity of 1 g of sample (as a fine powder), including both washcoat and substrate, was loaded into the reactor. After being oxidized at 400 °C in 10% O_2/He for 15 min, followed by reduction at 300 °C in 10% H_2/Ar for 15 min, the catalyst was heated up to 400 °C (hold time 10 min) in flowing Ar to remove adsorbed H. Pulsed H_2 chemisorption was initiated using a four-way valve after the catalyst had been cooled to -78 °C. During this measurement, 0.5 ml of 10% H_2/Ar was pulsed into the reactor every 2 min, the H_2 signal at the reactor outlet being monitored with a thermal conductivity detector (TCD). H_2 pulsing was terminated after the TCD signal had reached a constant value i.e., the precious metal (Pt + Rh) sites were saturated with H_2. Assuming a 1:1 ratio of atomic hydrogen to surface Pt or Rh, the metal dispersion was calculated based on the amount of H adsorbed.

Materials for electron microscopy analysis were collected by scraping a small amount of washcoat from the catalyst monoliths and supporting them on TEM grids obtained from Electron Microscopy Sciences. Transmission electron microscopy (HR-TEM) and scanning transmission electron microscopy (STEM) investigations were conducted using a field emission JEOL 2010F STEM outfitted with a URP pole piece, GATAN 2000 GIF, GATAN DigiScann II, Fischione HAADF STEM detector, Oxford energy-dispersive X-ray detector and EmiSpec EsVision software. STEM measurements were acquired for fresh and aged samples using a high-resolution probe at 2 Å.

Temperature programmed reduction (TPR) experiments were conducted using a Micromeritics AutoChem II chemisorption analyzer, equipped with a thermal conducitivty (TCD) detector. 0.1 g of ground Cu-CHA catalyst was pretreated at 500 °C for 2 h under a flow of 10% O_2/Ar (50 ml/min), after which the sample was cooled to room temperature in flowing Ar. The sample was then purged in He for 1 h at RT until the TCD signal stabilized, after which TPR was performed in 1% H_2/Ar (60 ml/min) at a heating rate of 10 °C/min from RT to 800 °C.

Temperature-programmed NH_3 desorption experiments were performed in a microreactor using a mass spectrometer (Pfeiffer Thermostar GSD301) as the detector. Prior to measurements, the powder sample (ca. 0.15 g) was pretreated in flowing 10% O_2/He (40 ml/min) at 150 °C for 1 h and then purged with He (40 ml/min) with cooling to 100 °C. Samples were then exposed to 1% NH_3/He (40 ml/min) at 100 °C for 1 h, followed by purging with He (40 ml/min) for 2 h to remove physically adsorbed NH_3. Subsequently, the samples were heated to 700 °C under He (40 ml/min) at a ramp rate of 10 °C/min.

X-ray absorption spectroscopy (XAS) on references (Cu foil, Cu_2O, CuO, $Cu(OH)_2$ and $CuSO_4$) and catalyst samples before and after aging was conducted at Brookhaven National Laboratory (Beamline X-18b). The beamline was equipped with a Si (1 1 1) channel cut monochromator. A crystal detuning procedure was used to remove harmonic content from the beam and make the relative response of the incident and transmission detectors more linear. The X-ray flux for the beamline was ca. 1×10^{10} photons per second at 100 mA and 2.8 GeV; the usable energy range was from 5.8 to 40 keV. XAS spectra were recorded in transmission mode near the Cu K edge (8979 eV). Sample thickness was determined by calculating the amount in grams per square centimeter of sample as described elsewhere [37]. Boron nitride was utilized to dilute the sample, such that the wafer could be self-supported. EXAFS data

reduction was carried out using the WinXAS program [38]. The pre-edge background was removed with a linear function and the post-edge background was subtracted with a cubic spline method.

3. Results and discussion

3.1. N_2 physisorption, H_2 chemisorption, residual sulfur and X-ray diffraction analysis

N_2 physisorption data for the fresh and aged LNT and SCR catalysts are shown in Table 3. For both catalysts a significant drop in catalyst surface area is observed after aging. It should be noted that these values correspond to the presence of both the washcoat and catalyst substrate (cordierite). The loss of surface area and micropore volume is particularly significant for the SCR catalyst and suggests that after aging the zeolite pores are occluded to some degree. The results for the aged LNT catalyst are consistent with our earlier study, the observed increase in average pore diameter being indicative of a collapse of some of the smaller pores in the washcoat [29,30].

According to H_2 chemisorption measurements, aging resulted in severe sintering of precious metals (PMs) in the LNT, as evidenced by a significant drop in overall PM dispersion from 50.6% to 13.5%. In addition to sintering of the supported metals, the decrease in PM dispersion may also be the result of sintering of the CeO_2–ZrO_2 OSC material, which would result in some degree of PM encapsulation [39,40]. Given that Pt is believed to act as a conduit for NO_x spillover to and from the Ba phase, it follows that close proximity of Pt and Ba are required to achieve efficient NO_x storage and reduction. Pt sintering reduces the degree of Pt-Ba contact as reflected in the decreased interfacial perimeter (i.e., the total perimeter of all the Pt particles that are in contact with the Ba phase [30,41]), which, as past studies have shown, results in the deterioration of LNT performance [28–30].

Another effect associated with catalyst aging under simulated road conditions is the accumulation of sulfur in the washcoat. The results of sulfur analyses obtained for the aged catalysts are also collected in Table 3. Evidently, sulfur resided not only on the LNT but also on the SCR catalyst after aging. However, the amount of sulfur present in the LNT is higher than that in the SCR catalyst. This can be attributed to the formation bulk $BaSO_4$, which requires high temperatures ($\geq$750 °C) for its decomposition under rich conditions [27,30]. Due to the low sulfate concentration in the catalysts, XRD data (not shown) failed to show the presence of crystalline metal sulfates. Notably, the diffraction pattern of the Cu-CHA catalyst was unchanged after aging, indicating that the zeolite structure was retained.

3.2. Electron microscopy analysis of fresh and aged catalyst samples

According to STEM observations, in the fresh and aged LNT samples the alumina support occurred as agglomerates of spear-shaped crystals. Ba oxide was observed as a denser phase possessing a granular morphology, which appeared to coat the alumina in many places. Regions rich in ceria were also identified. Small platinum particles (~2 nm) associated with the alumina support appeared in both the fresh and aged LNT samples, while a high density of larger platinum particles was observed in the barium-rich areas in both samples. Particle sizes in the fresh LNT sample ranged in size up to ~13 nm, while platinum particles in the aged LNT sample grew as large as ~27 nm as a result of sintering (see Fig. 2). However, Pt associated with the alumina phase appeared to retain similar particle sizes to the fresh catalyst (~2 nm). EDS analysis (data not shown) confirmed the presence of sulfur in barium-rich areas after aging.

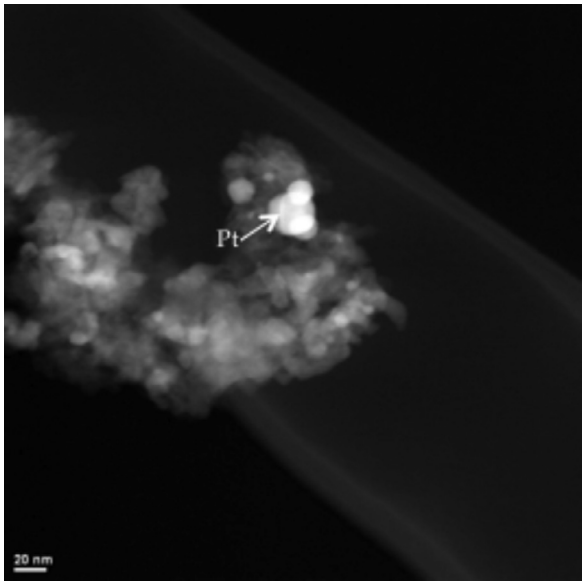

Fig. 2. STEM image of aged LNT catalyst showing three overlapping Pt particles.

TEM images of the fresh and aged Cu-CHA SCR catalyst are shown in Fig. 3. The fresh Cu-CHA catalyst consisted of crystallites with well-defined edges (Fig. 3a), whereas after aging the samples appeared to contain less well-defined structures; this suggests some loss of crystallinity (Fig. 3b), although this was not confirmed by XRD data. This apparent discrepancy is likely a reflection of the fact that whereas TEM analyzes only a small part of the sample, XRD is a bulk technique, i.e., the bulk of the sample retained a high degree of crystallinity. TEM analysis also revealed the presence of small CuO particles on the surface of the zeolite after aging; most of the particles fell in the 1–4 nm size range, although some larger particles (5–7 nm) were also present. This observation is consistent with reports that CuO crystallites form on the surface of Cu-SSZ-13 [34] after aging. Evidently, Cu^{2+} species initially located in the cage of the zeolite migrated to the outer surface and underwent agglomeration to form CuO nanoparticles. Indeed, the loss of micropore volume noted in Section 3.1 above may be attributed to the blocking of pore openings and channels by the formed CuO nanoparticles.

Notably, the maximum temperature experienced by the sample during aging was 750 ± 10 °C, for a total of 8.5 h. In the study by Schmieg et al. [34], extensive CuO nanoparticle formation was observed on a commercial Cu-CHA catalyst after 120 h of hydrothermal aging (under constant lean conditions) at 800 °C, resulting in significant degradation in catalyst performance. In the same study it was found that hydrothermal aging at 800 °C for 16 h resulted in little degradation in performance, an observation in agreement with other studies in which hydrothermal aging was performed at 800 °C for relatively short periods (12–16 h) [32,33]. The fact that in our study CuO nanoparticle formation was observed, together with some degradation in SCR performance (vide infra) – despite the lower aging temperature – suggests that exposure of the catalyst to alternating lean-rich conditions at 750 °C may have contributed to this degradation. Specifically, it can be envisaged that exposure of the catalyst to rich conditions at high temperatures results in reduction of Cu^{2+} ions to metallic Cu (as indicated by H_2-TPR data presented below), which should be more mobile than Cu^{2+} due to the absence of the strong electrostatic interaction with the zeolite framework. In this regard, a study of Cu-CHA aging behavior under rich conditions would be of interest.

Table 3
Physical properties of fresh and aged catalysts*.

Catalyst	Surface area (m^2/g)	Mesopore volume (cm^3/g)	Micropore volume (cm^3/g)	Average pore radius (nm)	Mean PM dispersion (%)	Aver.PM particle size (nm)	Residual sulfur (wt%)
Fresh-LNT	58.0	0.18	–	6.61	50.6	2.2	–
Aged-LNT	37.3	0.16	–	9.22	13.5	8.4	0.70
Fresh-SCR	203.9	0.12	0.08	9.60	–	–	–
Aged-SCR	109.4	0.06	0.04	9.94	–	–	0.30

* Surface area, mesopore volume and micropore volume values represent the average of the catalyst washcoat and the cordierite substrate.

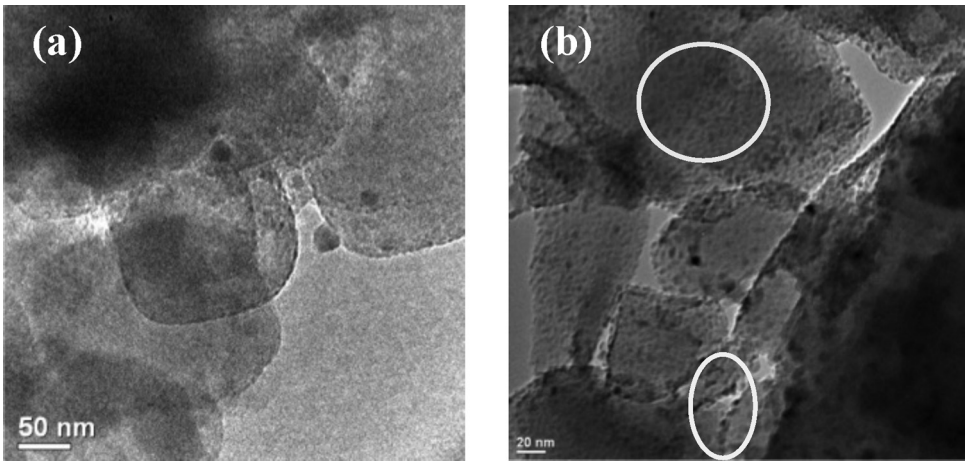

Fig. 3. (a) TEM image of fresh Cu-CHA catalyst; (b) TEM image of aged Cu-CHA catalyst. Areas rich in CuO nanoparticles are circled.

3.3. XANES measurements

The near-edge structure of X-ray absorption spectra collected at the Cu K edge for both reference compounds and catalysts is shown in Fig. 4. An increase of 1.0 eV in the edge energy was observed for Cu_2O as compared to metallic Cu, while a further increase was found when increasing Cu oxidation state from +1 (Cu_2O) to +2 (CuO), indicating that a higher energy is required to free the electron from the Cu K shell. For the same oxidation state, a slight shift of edge energy to higher position was observed when comparing CuO with $Cu(OH)_2$ (8.983 keV → 8.985 keV). Moreover, a further shift to higher energy was seen when sulfur (as sulfate) was attached to the O atoms instead of H. These findings confirm that XAS edge energy is sensitive to Cu oxidation state and coordination environment. On this basis, both the fresh and aged Cu-chabazite catalysts were investigated at the Cu K-edge. As shown in Fig. 4, the fresh Cu-chabazite catalyst displayed an edge energy of 8.987 keV, being the highest among the samples investigated. As addressed by Ribeiro et al. [42], the edge energy can reach values as high as 8.989 keV when isolated Cu^{2+} is coordinated with H_2O. Therefore, this finding infers high coordination environment around isolated Cu^{2+} in the cage of the fresh Cu-chabazite. After aging, the edge energy decreased by 3 eV. This observation is consistent with TEM and TPR data which suggest that upon aging some of the Cu migrated out of the cage and aggregated to form CuO; the contribution of the formed CuO in XAS would be expected to lower the Cu edge energy. While the formation of $CuSO_4$ would not be expected to shift the energy edge by as much as CuO, it is apparent that on average their contributions caused a decrease in edge energy compared to the fresh counterpart. Moreover, the extent of decrease suggests that a significant amount of highly coordinated Cu^{2+} migrated out of cage to form CuO after aging.

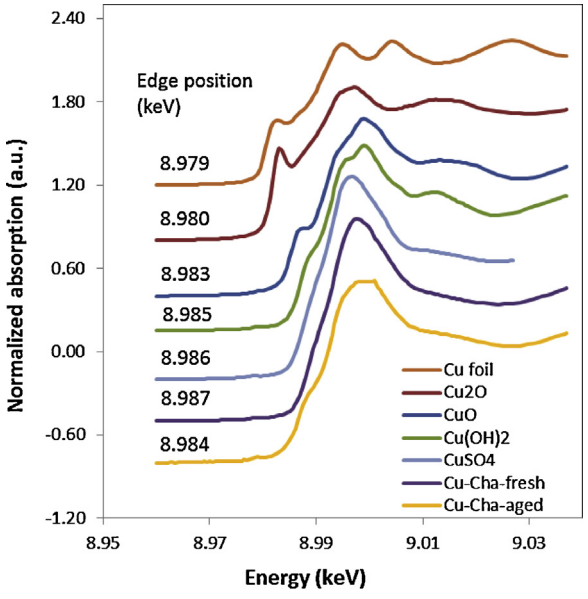

Fig. 4. X-ray absorption near-edge spectra of reference compounds and catalysts at Cu *K* edge. Reference compounds include Cu foil, Cu_2O, CuO, $Cu(OH)_2$, and $CuSO_4$. Catalysts include both fresh and aged Cu-chabazite.

3.4. NO_x storage on fresh and aged LNT catalysts

In order to study the effect of aging on the NO_x storage efficiency (NSE) of the LNT catalyst, a comparison between the initial and the cycle-averaged NSE was made, as shown in Fig. 5. Herein the NSE is defined as the fraction of NO_x fed that is stored in the lean phase. The NSE obtained in the first lean cycle (after complete catalyst regeneration at 500 °C) is regarded as the initial (or "first-cycle") NSE, whereas the NSE obtained in the lean phase under stationary cycling conditions is regarded as the "cycle-averaged" NSE. As shown, the fresh catalyst showed very high initial NSE values at the four temperatures tested, and only small differences were observed between them. The drop in NSE under subsequent cycling

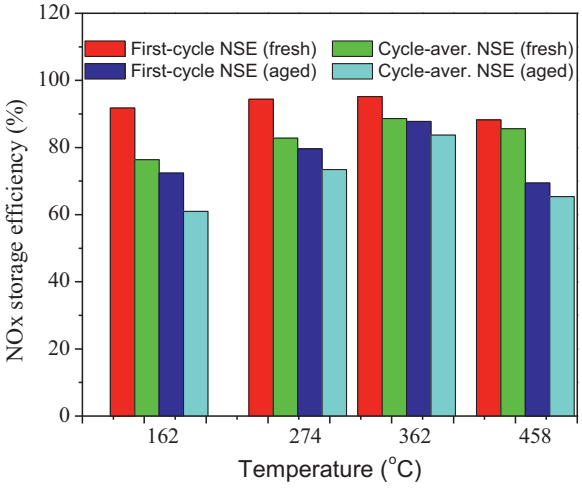

Fig. 5. Comparison of NO_x storage efficiency (NSE) during the first cycle and subsequent lean-rich cycling for fresh and aged LNT catalyst. Feed: lean (60 s): 500 ppm NO, 8% O_2, 5% CO_2, 5% H_2O, balance N_2; rich (5 s): 2.5% H_2, 5% CO_2, 5% H_2O, balance N_2. GHSV = 60,000 h^{-1}.

was observed to be slight at 362 and 458 °C, showing that the fresh catalyst was nearly fully regenerated at these temperatures. However, at the lower temperatures regeneration was not complete, as evidenced by a drop in NSE, due to the slow kinetics of NO_x release. After aging significant decreases in initial NSE were observed at all temperatures in the range 162–458 °C. As for our previous studies [29,30], this can be attributed to segregation of the Ba and Pt phases, as well as to the partial sulfation of the Ba NO_x storage phase, both of which result in less efficient NO_x storage. Interestingly, the relative difference between the first cycle and cycle-averaged NSE values at each measurement temperature for the aged catalyst was similar to that observed for the fresh catalyst. This suggests that even after aging, the LNT was able to maintain a reasonable balance between NO_x storage and reduction, i.e., the catalyst retained good activity for NO_x reduction. However, overall these findings point to an increase in lean phase NO_x slip from the aged LNT during lean-rich cycling.

3.5. Temperature programmed reduction of fresh and aged SCR catalysts

In order to examine the effects of aging on the nature of the Cu species in the SCR catalyst, H_2-TPR experiments were performed on the fresh and aged SCR catalysts. Fig. 6 shows the resulting H_2-TPR data. For the fresh catalyst, reduction maxima are observed at 230 and 450 °C. According to the literature [43], reduction maxima observed for Cu-SAPO-43 at 230 and 425 °C can be attributed to Cu^{2+} reduction to Cu^+ and to Cu^+ reduction to Cu^0, respectively. In the case of Cu-SSZ-13, Kwak et al. [32] report a main reduction peak at 230 °C, together with a broad shoulder at ca. 300 °C. These features were tentatively assigned to Cu^{2+} to Cu^+ reduction of ions located in type IV sites (inside the eight-membered ring connecting the CHA cavities) and type I sites (inside the CHA cavity), respectively. For the aged catalyst (Fig. 6), the peak at *ca.* 450 °C is still present, while the lower temperature peak is shifted to *ca.* 300 °C. While this shift suggests that migration of Cu^{2+} ions from one site type to the other has occurred, it should be noted that the reduction of CuO crystallites in a number of different zeolite structures has been reported to give rise to a reduction peak at *ca.* 300 °C [32,43]. Hence, the peak at 300 °C may represent a combination of these two features. Notably, a peak observed at 765 °C for the aged catalyst – which is not seen for the fresh catalyst – can be attributed to sulfate reduction.

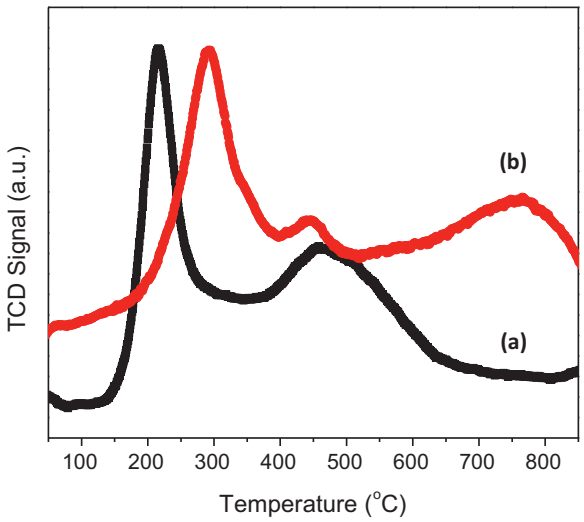

Fig. 6. H_2-TPR profiles for (a) fresh and (b) aged Cu-CHA catalysts.

3.6. Temperature programmed desorption of NH_3 from fresh and aged SCR catalysts

Fig. 7 shows the NH_3 temperature programmed desorption (TPD) profile for the fresh and aged SCR catalysts. The fresh SCR catalyst has three peaks, which are centered at 185, 304, and 498 °C, respectively. According to the work of Hong and co-workers [44], the first and third peaks can be attributed to desorption of ammonia species from weak acid (Lewis acid) sites and strong acid (Brønsted acid) sites in SSZ-13, respectively [44]. Amin et al. [45] have reported that the introduction of Cu into ZSM-5 by an ion-exchange method creates medium-strength acid sites. Although the caveat must be added that ZSM-5 is structurally different from SSZ-13, nonetheless the presence of the second TPD peak at 304 °C can logically be ascribed to ammonia desorption from such medium-strength Cu sites (given the propensity of Cu ions to coordinate NH_3). Upon aging the SCR catalyst, the intensity of all three TPD peaks decreased, the decrease being most pronounced for the strong Brønsted acid sites. Quantification of the NH_3 revealed a decrease in the amount of NH_3 desorbed from 0.30 mmol/g for the fresh catalyst to 0.14 mmol/g after aging. These results suggest

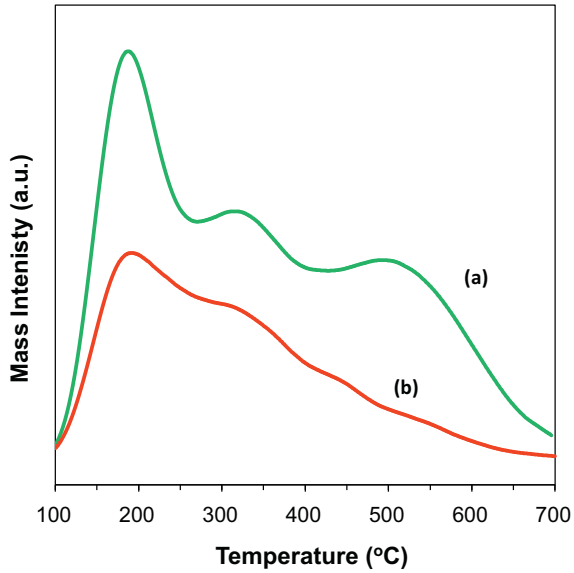

Fig. 7. NH_3-TPD profiles of (a) fresh and (b) aged Cu-CHA catalysts.

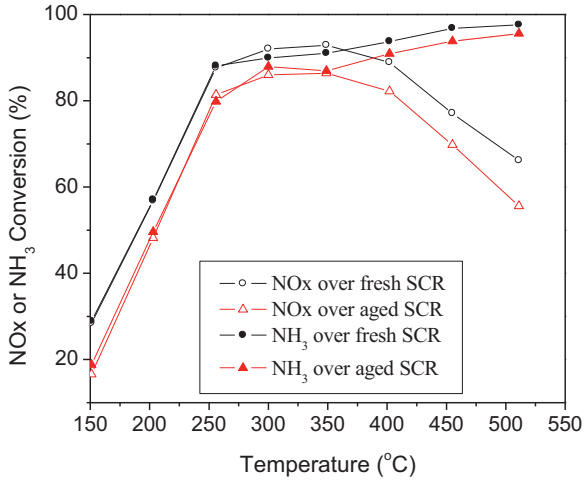

Fig. 8. NO_x and NH_3 conversion over fresh and aged Cu-CHA catalysts as a function of temperature under continuous flow conditions.

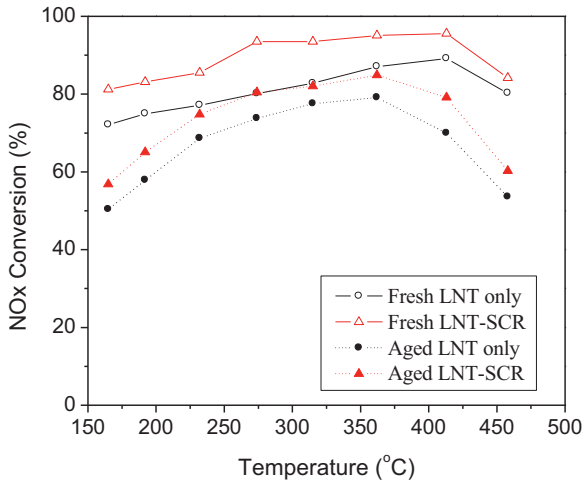

Fig. 9. Comparison of cycle-averaged NO_x conversion over LNT catalyst and LNT–SCR system using 2.5% H_2 as reductant.

that the three site types are to some degree converted into sites that do not adsorb ammonia. In the case of the medium-strength sites, the implication is that these are Cu^{2+} (Lewis acid) sites which after aging are reduced in number due to the formation of CuO nanoparticles and/or due to the presence of sulfate (which occupies coordination sites on the Cu^{2+} ions). It is well accepted that the acidic properties of zeolite-like SCR catalysts represent a crucial factor that determines NH_3 adsorption capacity and affects NO_x reduction activity [46]. Hence, based on the NH_3-TPD profile of the aged catalyst, some deterioration in the NH_3-SCR activity of the catalyst can be expected.

3.7. Catalytic activity of fresh and aged Cu-CHA catalysts for SCR of NO_x by NH_3

From the above analytical data, it is evident that the Cu-CHA catalyst undergoes structural changes during aging. In order to assess whether these changes affect the NH_3-SCR activity of the catalyst, steady-state NO_x reduction experiments were performed over the fresh and aged catalysts. As shown in Fig. 8, for both catalysts the NO_x conversion is observed to peak in the range 300–350 °C. At higher temperatures the NO_x conversion decreases, while the NH_3 conversion continues to increase. This is indicative of the fact that at higher temperatures NH_3 oxidation by O_2 becomes competitive with the NH_3-SCR reaction, thereby limiting the NO_x conversion [47]. The NH_3 and NO_x conversion trends are very similar for the fresh and aged catalysts, although after aging, the NO_x conversion decreased by 8–10% (absolute) across the entire temperature range tested. The NH_3 conversion is also decreased after aging by a similar amount, although it is noticeable that the NH_3 conversion is less affected by aging in the higher temperature range, suggesting that NH_3 oxidation by O_2 is less sensitive to the effects of catalyst aging than the NH_3-SCR reaction.

3.8. Fresh and aged LNT–SCR system behavior under lean-rich cycling

3.8.1. 2.5% H_2 as reductant

Fig. 9 shows a comparison of the cycle-averaged NO_x conversions obtained for the fresh and aged LNT–SCR systems when using 2.5% H_2 as the rich phase reductant (rich phase condition 1 in Table 2). Note that each set of LNT-only and LNT–SCR results correspond to one experiment, i.e., the LNT-only results are based on the gas composition measured between the LNT and SCR catalysts. As shown in Fig. 9, before aging the LNT–SCR system affords about 10% higher NO_x conversion levels across the entire temperature window examined (150–450 °C). After aging, the LNT catalyst is significantly deactivated, the peak NO_x conversion decreasing from ca. 90% to 80%, while NO_x conversion in the low (<225 °C) and high (>375 °C) temperature regions is more severely affected. After aging the benefit resulting from the presence of the SCR catalyst is still evident across the entire temperature range.

It is well known that NH_3 generated from an LNT during rich phase purging can be stored on a downstream SCR catalyst, such that it can react with NO_x slip during the subsequent lean phase [11–20]. Moreover, a number of studies [29,30,48–51] have reported that the LNT selectivity to NH_3 is typically increased after aging. There are several factors which can contribute to this phenomenon. For instance, relative to the fresh LNT, the higher ratio of H_2 to stored NO_x for the aged LNT (due to its lowered NO_x storage capacity), should result in increased production of NH_3 [48]. Moreover, lengthening of the NO_x storage-reduction zone (due to the lower NO_x storage capacity per unit length of catalyst), results in decreased NH_3 consumption by NO_x and O_2 downstream of the reductant front [48–51]. In addition, higher intracatalyst NH_3 concentrations measured after aging by spatially resolved capillary inlet mass spectrometry (spaciMS) [50,51] indicate that selectivity to NH_3 is increased as a consequence of the increased effective H_2: NO_x ratio at the precious metal sites; this, in turn, is the result of the decreased rate of NO_x migration from storage sites to PGM centers (due to PGM/Ba phase segregation) relative to the rate of propagation of the reductant front [41,51,52].

In order to clarify the relationship between NH_3 production from the LNT and the benefit of the SCR catalyst with respect to NO_x conversion, the product selectivities for the LNT catalyst and the combined LNT–SCR system are compared in Fig. 10. These data confirm that the selectivity to NH_3 over the LNT is increased after aging. For example, the selectivity to NH_3 over the fresh LNT is 30.1%, 21.4% and 12.1% at, respectively, 192, 274 and 413 °C. After aging, these values increase to 47.0%, 28.8% and 18.8%, respectively. Combining these data with the results shown in Fig. 9, the increased NO_x conversion over the aged SCR catalyst can be rationalized on the basis that more NO_x and NH_3 are available for reaction on the SCR catalyst after aging. The exact amounts NH_3 and NO_x converted across the SCR catalyst will be discussed below.

It is also noteworthy that a decrease in the selectivity of NO_x reduction to N_2O is observed over the LNT catalyst after aging; moreover, N_2O so generated is partly mitigated by the downstream SCR catalyst. This result is consistent with our recent study [26], in

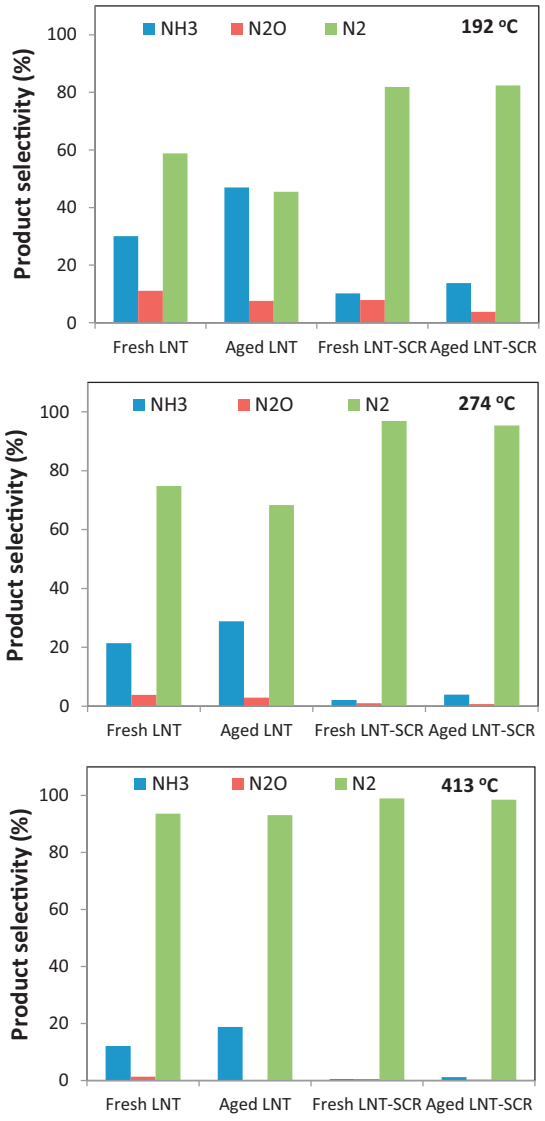

Fig. 10. Comparison of product selectivity over LNT catalyst and LNT–SCR system using 2.5% H_2 as reductant; top: 192 °C; middle: 274 °C; bottom: 413 °C.

which Cu-CHA was found to catalyze the decomposition of N_2O. In the presence of reductants which slip through the LNT (H_2, NH_3, etc.), the rate of N_2O decomposition is greatly increased [26]. Evidently, after aging, the SCR catalyst remained active for N_2O decomposition.

The amounts of NO_x and NH_3 converted across the SCR catalyst are shown in Table 4. From this it is apparent that at each temperature the absolute amount of NO_x converted over both the fresh and aged SCR catalysts is lower than the amount of NH_3 converted. This is consistent with the typical mechanism for NO_x performance improvement in coupled LNT–SCR systems, i.e., NH_3 slip from the LNT is stored on the SCR catalyst and reacts with sequential lean phase NO_x slip to form N_2. The additional NH_3 consumption can be attributed to its oxidation over the SCR catalyst.

3.8.2. 2.5% CO as reductant

Fig. 11 compares NO_x conversion as a function of temperature for the fresh and aged LNT–SCR systems when using 2.5% CO as the reductant (rich phase condition 2 in Table 2). The deactivation of the aged LNT catalyst is again evident, the peak NO_x conversion decreasing from ca. 85% to 70%. While a small NO_x

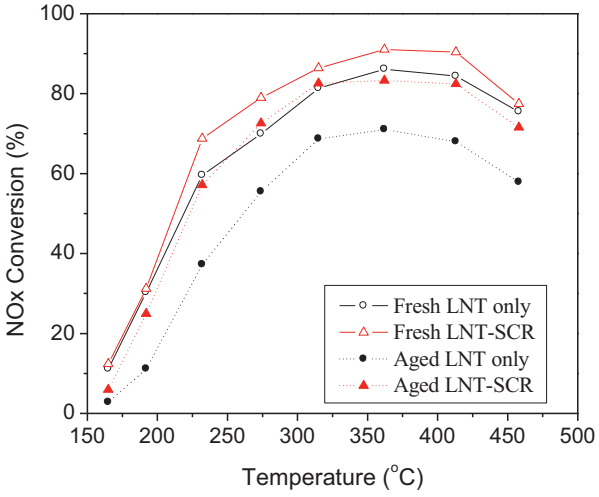

Fig. 11. Comparison of cycle-averaged NO_x conversion over LNT catalyst and LNT–SCR system using 2.5% CO as reductant.

conversion benefit is observed for the fresh LNT–SCR system over the corresponding LNT-only configuration, after aging this benefit becomes more apparent, especially at relatively higher temperatures (>230 °C), such that the increased NO_x conversion over the SCR catalyst helps to compensate for the decreased LNT NO_x reduction activity. These results again serve to highlight the synergy that exists between LNT and SCR catalysts.

Fig. 12 shows the product selectivity for the LNT catalyst and LNT–SCR systems using 2.5% CO as the reductant. As was the case for H_2, the selectivity of NO_x reduction to NH_3 over the LNT is increased after aging. It is also noteworthy that after aging a decrease in the selectivity of NO_x reduction to N_2O over the LNT catalyst is observed. The selectivity to N_2O is high at 192 °C for both the fresh and aged LNT when CO is used as the reductant, although the low NO_x conversion at this temperature limits the N_2O emission from the LNT in absolute terms. In general, the factors controlling the selectivity of NO_x reduction to N_2O are poorly understood, although catalyst composition appears to play a major role. The nature of the reductant has also been highlighted; however, published data are conflicting on the subject of which reductant affords the highest selectivity to N_2O [53–55]. This is presumably a consequence of differences in the composition of the catalysts used in these studies, as well as the use of different reaction conditions. As shown in Fig. 12, the magnitude of the decrease in N_2O selectivity after aging is significant; moreover, the aged SCR catalyst continues to catalyze the decomposition/reduction of a portion of the N_2O emitted by the LNT catalyst.

Table 5 shows the amounts of NO_x and NH_3 converted across the SCR catalyst. Notably, for both the fresh and aged SCR catalyst, the amount of NO_x converted exceeds the amount of NH_3 converted. In our earlier study [25] we observed similar behavior when using propene or ethene as the NO_x reductant and showed that hydrocarbon slip from the LNT catalyst contributed to the NO_x reduction observed over the SCR catalyst. Evidently, similar behavior can occur with CO. This is unsurprising given the reported ability of Cu-ZSM-5 to catalyze NO_x reduction with CO. In the absence of oxygen CO is an excellent NO_x reductant over Cu-ZSM-5 [56], whereas in the presence of oxygen NO_x reduction is largely suppressed, CO oxidation by O_2 being the dominant pathway [56,57]. In steady-state tests, we have observed that the Cu-CHA catalyst used in the present study shows similar behavior with respect to NO reduction by CO, although as shown in Fig. S2 (supplementary data), even in the presence of excess O_2 some NO_x reduction is observed at the feed CO concentration of 2.5% used in this study.

Table 4
Comparison of NO_x and NH_3 conversion over SCR catalyst in LNT–SCR system using 2.5% H_2 as reductant.

Catalyst	T (°C)	NO_x converted (μmol)	% NO_x from LNT converted	NH_3 converted (μmol)	% NH_3 conversion	NH_3 converted–NO_x converted (μmol)
Fresh	192	10.2	21.8	15.7	38.1	5.5
Aged	192	19.3	22.3	21.4	36.5	2.1
Fresh	274	24.1	58.9	37.0	91.1	12.9
Aged	274	29.6	60.4	45.2	88.7	15.6
Fresh	413	6.9	33.9	22.0	96.2	15.1
Aged	413	19.5	34.8	23.2	95.8	3.7

Table 5
Comparison of NO_x and NH_3 conversion over SCR catalyst in LNT–SCR system using 2.5% CO as reductant.

Catalyst	T (°C)	NO_x converted (μmol)	% NO_x from LNT converted	NH_3converted (μmol)	% NH_3conversion	NH_3 converted–NO_x converted (μmol)
Fresh	192	11.7	9.0	1.7	28.0	−10.0
Aged	192	15.9	9.6	1.8	27.8	−14.1
Fresh	274	16.9	30.1	15.1	76.1	−1.8
Aged	274	32.0	38.5	16.6	74.9	−15.4
Fresh	413	11.3	38.5	10.8	90.5	−0.5
Aged	413	24.9	41.7	10.7	86.6	−14.2

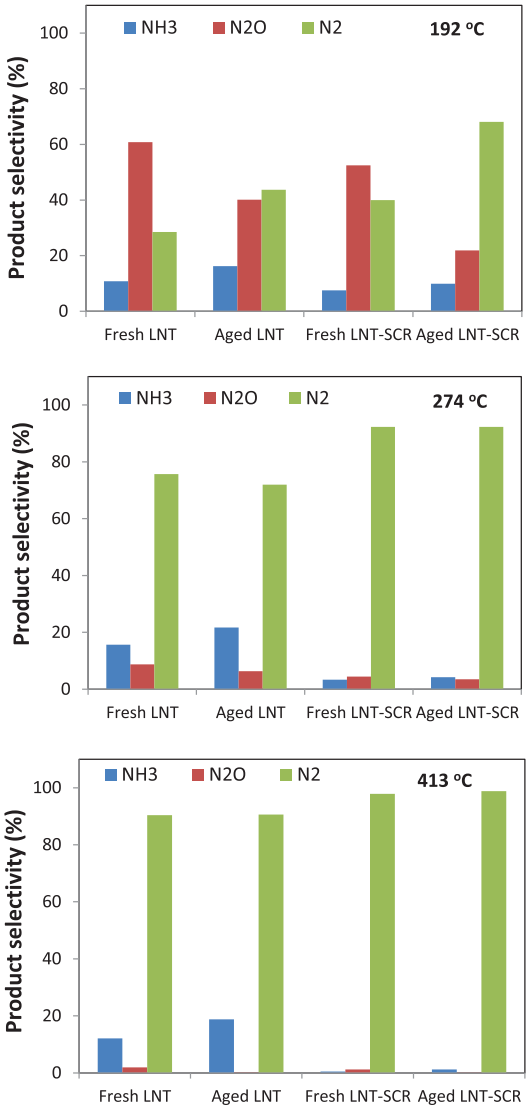

Fig. 12. Comparison of product selectivity over LNT catalyst and LNT–SCR system using 2.5% CO as reductant; top: 192 °C; middle: 274 °C; bottom: 413 °C.

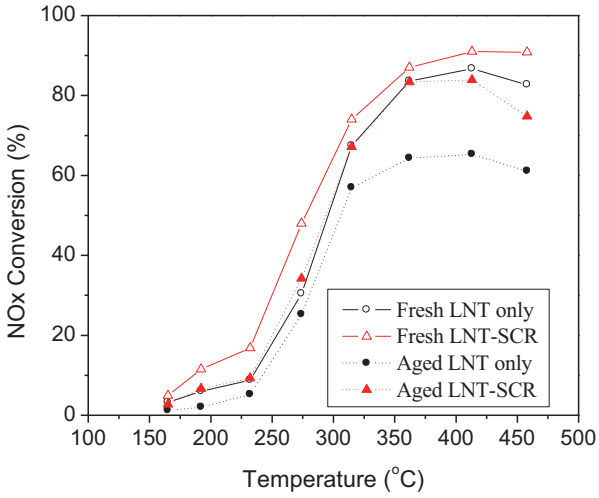

Fig. 13. Comparison of cycle-averaged NO_x conversion over LNT catalyst and LNT–SCR system using 3333 ppm C_3H_6 as reductant.

However, preliminary data (not shown) indicate that under lean-rich cycling NO_x reduction by CO is significant under rich conditions only. This could be due to a low storage capacity of Cu-CHA for CO (as compared to olefins), and/or due to CO desorption/oxidation after the switch to lean conditions. In contrast, slipped propene and ethene from the LNT are adsorbed in the Cu-CHA catalyst during rich purging, and are available for reaction with NO_x both in the rich phase and for a significant period of the subsequent lean operation [24].

3.8.3. 3333 ppm C_3H_6 as reductant

The NO_x conversion during cycling for the fresh and aged LNT–SCR systems using 3333 ppm C_3H_6 (rich phase condition 3 in Table 2) is shown in Fig. 13. After aging, NO_x reduction over the LNT decreased, particularly over the temperature range 300–450 °C, although again the SCR catalyst compensated for the loss of NO_x conversion over LNT to a significant degree; indeed, the aged LNT–SCR system achieved similar NO_x conversion to the fresh LNT catalyst. The product selectivity displayed by the fresh and aged LNT is shown in Fig. S3. From these data, it can be seen that NO_x reduction selectivity to NH_3 increased with increasing temperature over both the fresh and aged LNT. Moreover, after aging the NH_3 selectivity was increased at each temperature. These results are in agreement with an earlier study [50], in which it was found that

Table 6
Comparison of NO_x and NH_3 conversion over SCR catalyst in LNT–SCR system using C_3H_6 as reductant.

Catalyst	T (°C)	NO_x converted (μmol)	% NO_x from LNT converted	NH_3 converted (μmol)	% NH_3 conversion	NH_3 converted–NO_x converted (μmol)
Fresh	192	3.2	1.8	0.0	0.0	−3.2
Aged	192	3.8	2.1	0.0	0.0	−3.8
Fresh	274	15.0	10.7	1.1	73.3	−13.9
Aged	274	18.9	11.8	1.5	69.5	−17.4
Fresh	413	12.4	30.4	11.2	96.7	−1.2
Aged	413	18.8	31.9	15.7	93.4	−3.1

the C_3H_6 steam reforming activity of a fully formulated LNT catalyst increased with increasing temperature; the resulting CO and H_2 can function as in situ NO_x reductants, with the formation of NH_3 at high temperatures (>350 °C).

The amounts of NO_x and NH_3 converted across the SCR catalyst are listed in Table 6. These results highlight the fact that relatively small amounts of NH_3 are produced by the LNT, nearly all of which is converted over the SCR catalyst at high temperatures. However, in each case the amount of NO_x converted over the SCR catalyst consistently exceeds the NH_3 converted. For example, at 274 °C the amount of NO_x converted over the fresh and aged SCR catalyst (15.0 and 18.9 μmol, respectively) greatly exceeds the NH_3 converted (1.1 and 1.5 μmol, respectively). Although the amount of NH_3 generated from both the fresh and aged LNT catalyst is greatly increased upon increasing the temperature to 413 °C, the amount of NO_x converted across SCR is still higher than that of NH_3 converted. As for the results obtained when using CO as the reductant (see above), and as for our previous study using propene and ethene as reductants in a fresh (i.e., degreened) LNT–SCR system [24], these observations are consistent with the utilization of the reductant by the SCR catalyst.

It is also notable that the SCR catalyst contributes to the mitigation of hydrocarbon slip from the LNT. This can occur via the reaction of C_3H_6 with NO_x during the rich phase, as well as via its reaction with O_2 or NO_x in the lean phase (as a consequence of its storage by the zeolite). Table S1 shows the C_3H_6 conversion over the fresh and aged LNT and SCR catalysts. As expected, C_3H_6 conversion over both catalysts is strongly temperature dependent, increasing with increasing temperature. After aging, C_3H_6 conversion over both catalysts is notably decreased, although the SCR catalyst continues to show a modest benefit in terms of converting the hydrocarbon slip from the LNT.

Finally, it is of interest to compare the benefit in system NO_x conversion provided by the SCR catalyst after aging. Fig. 14 shows the difference in NO_x conversion for the aged LNT and LNT–SCR configurations as a function of temperature for the three reductants used in this study. Clearly, the greatest benefit is obtained when CO and C_3H_6 are the reductants. This is explained by the fact that the LNT catalyst is unable to utilize these reductants as efficiently as H_2 due to their lower reactivity; hence, more NO_x and reductant slip reaches the SCR catalyst. The ability of the SCR catalyst to utilize these reductants therefore provides a significant advantage over the LNT-only configuration. It is also notable that in the case of propene, the greatest benefit is obtained at ~350–400 °C, which corresponds both to the optimum temperature range for the HC-SCR reaction [21], and the temperature range over which steam reforming of propene typically lights off over Pt/Rh LNT catalysts [50], in turn resulting in increased NH_3 formation over the LNT.

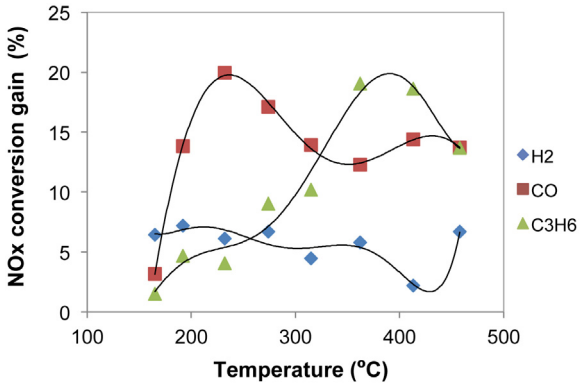

Fig. 14. Gain in system NO_x conversion for LNT–SCR configuration compared to LNT catalyst after aging.

4. Conclusions

Analysis of LNT and SCR catalysts subjected to simulated road aging revealed, in the case of the LNT, two main physico-chemical changes which contributed to catalyst deactivation: the accumulation of sulfur associated with the Ba phase, and sintering of the precious metals, resulting in decreased contact between the Pt and Ba phases. In the case of the SCR catalyst, upon aging some fraction of the Cu^{2+} species initially located in the zeolite migrated to the outer surface and underwent agglomeration to form CuO nanoparticles, although the catalyst maintained a high degree of activity in the NH_3-SCR reaction. Reactor tests showed that the aged LNT possessed decreased activity for NO_x storage and reduction, while exhibiting increased selectivity to NH_3 in the temperature range 150–450 °C. NH_3 generated from the LNT was stored by the SCR catalyst which subsequently catalyzed its reaction with NO_x slip from the LNT. Hence, the loss of NO_x conversion over the LNT was partly compensated by the downstream SCR catalyst.

The results of this study illustrate the promise of coupled LNT–SCR systems for the mitigation of NO_x emissions from lean-burn engines. In addition to compensating for decreased LNT activity after aging, the coupled LNT–SCR approach was found to possess several other advantages as compared with the LNT-only configuration:

- Under lean-rich cycling conditions, N_2O emissions from the LNT were partially mitigated by the downstream SCR catalyst.
- In addition to catalyzing NO_x reduction with NH_3 formed over the LNT, the Cu-CHA SCR catalyst was able to utilize slipped CO or C_3H_6 as NO_x reductants.
- Due to the ability of Cu-CHA to store C_3H_6 slip from the LNT and subsequently catalyze its reaction with NO_x or O_2, hydrocarbon emissions were lower from the LNT–SCR system than the LNT-only system.

Disclaimer

service by trade name, trademark, manufacturer, or otherwise does not necessarily constitute or imply its endorsement, recommendation, or favoring by the United States Government or any agency thereof. The views and opinions of authors expressed herein do not necessarily state or reflect those of the United States Government or any agency thereof.

Acknowledgements

This project was funded by the U.S. Department of Energy (DOE) under award No. DE-EE0000205. The authors thank BASF for providing the catalysts used in this study.

Appendix A. Supplementary data

Supplementary data associated with this article can be found, in the online version, at http://dx.doi.org/10.1016/j.apcatb.2013.10.037.

References

[1] H. Hu, J. Reuter, J. Yan, J. McCarthy Jr., SAE Technical Paper 2006-01-3552, 2006.
[2] K.E. Bevan, W. Taylor III, SAE Technical Paper 2006-01-3551, 2006.
[3] R. Roecker, R. Zhan, R.H. Stanglmaier, SAE Technical Paper 2007-01-3983, 2007.
[4] R. Snow, G. Cavatatio, D. Dobson, C. Montreuil, R. Hammerle, SAE Technical Paper 2007-01-1244, 2007.
[5] R. Snow, D. Dobson, R. Hammerle, S. Katare, SAE Technical Paper 2007-01-0469, 2007.
[6] T. Nakatsuji, M. Matsubara, J. Rouistenmäki, N. Sato, H. Ohno, Appl. Catal., B 77 (2007) 190.
[7] H. Shinjoh, N. Takahashi, K. Yokota, Top. Catal. 42–43 (2007) 215.
[8] X. Chen, J. Schwank, Top. Catal. 46 (2007) 39.
[9] E.C. Dykes, SAE Technical Paper 2008-01-2642, 2008.
[10] E.C. Corbos, M. Haneda, X. Courtois, P. Marecot, D. Duprez, H. Hamada, Appl. Catal., A 365 (2009) 187.
[11] L. Xu, R. McCabe, W. Ruona, G. Cavataio, SAE Technical Paper 2009-01-0285, 2009.
[12] M. Weibel, N. Waldbüsser, R. Wunsch, D. Chatterjee, B. Bandl-Konrad, B. Krutzsch, Top. Catal. 52 (2009) 1702.
[13] R. Zukerman, L. Vradman, M. Herskowitz, E. Liverts, M. Liverts, A. Massner, M. Weibel, J.F. Brilhac, P.G. Blakeman, L.J. Peace, Chem. Eng. J. 155 (2009) 419.
[14] L. Xu, R. McCabe, M. Dearth, W. Ruona, SAE Technical Paper 2010-01-0305, 2010.
[15] D. Chatterjee, P. Koči, V. Schmeisser, M. Marek, M. Weibel, B. Krutzsch, Catal. Today 151 (2010) 395.
[16] R. Bonzi, L. Lietti, L. Castoldi, P. Forzatti, Catal. Today 151 (2010) 376.
[17] P. Forzatti, L. Lietti, Catal. Today 155 (2010) 131.
[18] A. Lindholm, H. Sjövall, L. Olsson, Appl. Catal., B 98 (2010) 112.
[19] B. Pereda-Ayo, D. Duraiswami, J.R. González-Velasco, Catal. Today 172 (2011) 66.
[20] L. Castoldi, R. Bonzi, L. Lietti, P. Forzatti, S. Morandi, G. Ghiotti, S. Dzwigaj, J. Catal. 282 (2011) 128.
[21] J. Wang, Y. Ji, Z. He, M. Crocker, M. Dearth, R.W. McCabe, Appl. Catal., B 111–112 (2012) 562.
[22] Y. Liu, M.P. Harold, D. Luss, Appl. Catal., B 121–122 (2012) 239.
[23] L. Xu, R. McCabe, P. Tennison, H.-W. Jen, SAE Technical Paper 2011-01-0308, 2011.
[24] L. Xu, R.W. McCabe, Catal. Today 184 (2012) 83.
[25] Y. Liu, Y. Zheng, M.P. Harold, D. Luss, Appl. Catal., B 132 (2013) 293.
[26] J. Wang, M. Crocker, Catal. Lett. 142 (2012) 1167.
[27] W.S. Epling, L.E. Campbell, A. Yezerets, N.W. Currier, J.E. Parks II, Catal. Rev. 46 (2004) 163.
[28] D.H. Kim, Y.-H. Chin, G.G. Muntean, A. Yezeretz, N.W. Currier, W.S. Epling, H.-Y. Chen, H. Hess, C.H.F. Peden, Ind. Eng. Chem. Res. 45 (2006) 8815.
[29] Y. Ji, C. Fisk, V. Easterling, U. Graham, A. Poole, M. Crocker, J.-S. Choi, W. Partridge, K. Wilson, Catal. Today 151 (2010) 362.
[30] Y. Ji, V. Easterling, U. Graham, C. Fisk, M. Crocker, J.-S. Choi, Appl. Catal., B 103 (2011) 413.
[31] D.W. Fickel, E. D'Addio, J.A. Lauterbach, R.F. Lobo, Appl. Catal., B 102 (2011) 441.
[32] J.H. Kwak, D. Tran, S.D. Burton, J. Szanyi, J.H. Lee, C.H.F. Peden, J. Catal. 287 (2012) 203.
[33] Q. Ye, L. Wang, R.T. Yang, Appl. Catal., A 427–428 (2012) 24.
[34] S.J. Schmieg, S.H. Oh, C.H. Kim, D.B. Brown, J.H. Lee, C.H.F. Peden, D.H. Kim, Catal. Today 184 (2012) 252.
[35] C.K. Seo, H. Kim, B. Choi, M.T. Lim, C.H. Lee, C.B. Lee, Catal. Today 164 (2011) 507.
[36] V. Perrichon, L. Retailleau, P. Bazin, M. Daturi, J.C. Lavalley, Appl. Catal., A 260 (2004) 1.
[37] C. Shi, Y. Ji, U.M. Graham, G. Jacobs, M. Crocker, Z. Zhang, Y. Wang, T.J. Toops, Appl. Catal., B 119–120 (2012) 183.
[38] T. Ressier, J. Synchrotron Radiat. 8 (2001) 314.
[39] F. Fajardie, J.-F. Tempere, J.-M. Manoli, O. Touret, G. Djéga-Mariadassou, Catal. Lett. 54 (1998) 187.
[40] G.W. Graham, H.-W. Jen, W. Chun, R.W. McCabe, J. Catal. 182 (1999) 228.
[41] R.D. Clayton, M.P. Harold, V. Balakotaiah, C.Z. Wan, Appl. Catal., B 90 (2009) 662.
[42] V.F. Kispersky, A.J. Kropf, F.H. Ribeiro, J.T. Miller, Phys. Chem. Chem. Phys. 14 (2012) 2229.
[43] J. Xue, X. Wang, G. Qi, J. Wang, M. Shen, W. Lei, J. Catal. 297 (2013) 56.
[44] H. Jeon, C. Shin, H. Jung, S. Hong, Appl. Catal., A 305 (2006) 70.
[45] N. Amin, D. Anggoro, J. Nat. Gas Chem. 12 (2003) 123.
[46] L. Ren, Y. Zhang, S. Zeng, L. Zhu, Q. Sun, H. Zhang, C. Yang, X. Meng, X. Yang, F.-s. Xiao, Chin. J. Catal. 33 (2012) 92.
[47] P.S. Metkar, M.P. Harold, V. Balakotaiah, Chem. Eng. Sci. 87 (2013) 51.
[48] J-S. Choi, W.P. Partridge, J.A. Pihl, Mi-Y. Kim, P. Kočí, C.S. Daw, Catal. Today 184 (2012) 20.
[49] J-S. Choi, W.P. Partridge, J.A. Pihl, C.S. Daw, Catal. Today 136 (2008) 173.
[50] J. Wang, Y. Ji, V. Easterling, M. Crocker, M. Dearth, R.W. McCabe, Catal. Today 175 (2011) 83.
[51] V. Easterling, Y. Ji, M. Crocker, M. Dearth, R.W. McCabe, Appl. Catal., B 123 (2012) 339.
[52] D. Bhatia, M.P. Harold, V. Balakotaiah, Catal. Today 151 (2010) 314.
[53] H. Abdulhamid, E. Fridell, M. Skoglundh, Top. Catal. 30/31 (2004) 161.
[54] U. Elizundia, D. Duraiswami, B. Pereda-Ayo, R. Lopez-Fonscea, J.R. Gonzalez-Velasco, Catal. Today 176 (2011) 324.
[55] P. Koči, S. Bártová, D. Mráček, M. Marek, J.-S. Choi, M.-Y. Kim, J.A. Pihl, W.P. Partridge, Top. Catal. (2013), available at: DOI 10.1007/s11244-013-9939-y.
[56] M. Iwamoto, H. Hamada, Catal. Today 10 (1991) 57.
[57] J.L. d'Itri, W.M.H. Sachtler, Catal. Lett. 15 (1992) 289.